

Speckle noise in widefield radio-interferometry

H.K. Vedantham^{*} and L.V.E. Koopmans

Kapteyn Astronomical Institute, University of Groningen, P.O. Box 800, 9700 AV Groningen, The Netherlands

2 May 2022

ABSTRACT

In this paper we consider random phase fluctuations imposed during wave propagation through a turbulent plasma (e.g. ionosphere) as a source of additional noise in interferometric visibilities. We derive expressions for visibility variance for the wide field-of-view case (FOV ~ 10 deg) by computing the statistics of Fresnel-diffraction from a stochastic plasma, and provide an intuitive understanding. For typical ionospheric conditions (diffractive scale $\sim 5 - 20$ km at 150 MHz), we show that the resulting ionospheric ‘speckle noise’ can be a dominant source of uncertainty at low-frequencies ($\nu \lesssim 200$ MHz). Consequently, low-frequency ($\nu \lesssim 200$ MHz) widefield radio-interferometers must take this source of uncertainty into account in their sensitivity analysis. We also discuss the spatial, temporal, and spectral coherence-properties of speckle noise that determine its magnitude in deep integrations, and influence prospects for its mitigation via calibration or filtering.

Key words: methods: observational – techniques: interferometric – cosmology: dark ages, reionization, first stars

1 INTRODUCTION

Low frequency radio astronomy ($50 \text{ MHz} \lesssim \nu \lesssim 500 \text{ MHz}$) is currently generating significant interest from across astronomical disciplines (Taylor & Braun 1999). In a build-up to future telescopes like the SKA¹ and HERA² new pathfinder instruments like LOFAR (van Haarlem et al. 2013), MWA (Tingay et al. 2013), GMRT (Swarup et al. 1991), and PAPER (Parsons et al. 2010) are currently operational. Many of the science cases for these instruments demand unprecedented sensitivity levels. However, attaining the theoretical sensitivity limit (thermal noise) has been a perennial challenge at low frequencies ($\nu < 200 \text{ MHz}$). Low-frequency radio waves are corrupted during their propagation through plasma in the interstellar medium, interplanetary medium, and the Earth’s ionosphere. Understanding the ensuing propagation effects is critical not only to mitigate the resulting systematic errors, but also to study the media themselves. These plasma are known to be turbulent in nature and introduce a stochastic effect on radio-wave propagation. In this paper, we treat this inherent randomness³ as a source of uncertainty above and beyond the thermal noise. In doing so we show that visibility scintillation due to ionospheric propagation can be a dominant source of uncertainty at low frequencies ($\nu < 200 \text{ MHz}$). Without calibration/filtering of this noise, current and future instruments may not be able to attain their theoretical sensitivity limit.

Ionospheric-propagation effects are direction dependent, and have traditionally been mitigated using self-calibration (Pearson & Readhead 1984). Self-calibration is very effective on individual sources observed with a narrow field-of-view (FOV). With a wide FOV (several to tens of degrees) there may not be enough signal to noise ratio, or worse yet, enough constraints to solve for phase errors in different directions within the relevant phase decorrelation times-scales. This will invariably lead to direction dependent phase errors that give rise to speckle noise in visibilities. Such propagation effects have long been identified as ‘challenges’ to low-frequency wide-field observations, yet there has not been a concerted effort to evaluate the

^{*} E-mail: harish@astro.rug.nl

¹ Square Kilometre Array: visit <http://www.skatelescope.org> for details

² Hydrogen Epoch of Reionization Array: visit <http://reionization.org> for details

³ We will call this phenomena as ‘speckle-noise’ or ‘visibility scintillation’ after Cronyn (1972)

statistical properties of speckle noise— a primary aim of this paper.

Various aspects of radio-wave propagation through turbulent plasma have been studied since the discovery of radio-star scintillation (Smith 1950; Hewish 1952). Earlier theoretical work concentrated mainly on understanding intensity (zero-baseline) scintillations (Mercier & Budden 1962; Salpeter 1967). With the advent of VLBI (Very Long Baseline Interferometry) investigations into the general case of visibility scintillation were carried out (Cronyn 1972; Goodman & Narayan 1989). The above authors all assume a small FOV and compute the scintillation-statistics for a single source that is unresolved (or partially resolved) by the interferometer baseline— a case that is not relevant for current and future arrays with wide FOVs (several to tens of degrees). Recently, Koopmans (2010) has taken into account a wide FOV and a 3-dimensional ionosphere to study the ensemble averaged visibilities (infinite time-integration) that contain the speckle-halos or ‘seeing’ that develops around point-like radio sources. In this paper though, we are mainly concerned about the second-order visibility statistics (variance) and the associated time- frequency- and spatial-correlation properties for a wide FOV interferometer.

The rest of the paper is organised as follows. Section 2 describes the basic properties of a turbulent plasma and its effect on the wave-propagation phase. In Section 3, we compute the visibility statistics for a given (single) baseline due to phase modulation by the plasma. In Section 4, we use the results of Section 3 in conjunction with a realistic sky model to make forecasts for visibility scintillation due to ionospheric propagation. We choose the ionospheric case, since it is the dominant source of scintillation in current arrays, but we use a notation that is generic enough so as to be applicable also to inter-planetary and inter-stellar scintillation. In Section 5, we discuss the temporal, spatial, and spectral coherence of visibility scintillation— properties that are important to the evaluation of time/frequency averaging and aperture synthesis effects. Finally in Section 6 we present our salient conclusions, and draw recommendations for future work.

2 BASIC PROPERTIES

A turbulent plasma introduces a time, frequency, and position dependent propagation-phase on electromagnetic waves. These phase fluctuations are a direct consequence of density fluctuations in the plasma due to turbulence. Consequently, the propagation phase is expected to have certain statistical behaviour in time, frequency, and position. These statistical properties have been studied in detail elsewhere (see Wheelon (2001) and references therein), and we only summarise them here. For simplicity, we will assume the absence of an ordered magnetic field that may confine the plasma along preferred directions. We will also make use of the widely used ‘thin screen’ approximation (Wheelon 2003) wherein we assume the propagation phase in any given direction to be the integrated phase along that direction. This reduces the statistical description of plasma turbulence to an isotropic function in 2-dimensions.

2.1 Frequency dependence

The refractive index in a non-magnetised plasma is given by

$$\eta = \sqrt{1 - \frac{\nu_p^2}{\nu^2}} \approx 1 - \frac{1}{2} \frac{\nu_p^2}{\nu^2}, \quad (1)$$

where ν_p is the electron plasma frequency, ν is the electromagnetic-wave frequency, and the approximation holds for $\nu \gg \nu_p$. The plasma frequency itself is given by

$$\nu_p = \frac{1}{2\pi} \sqrt{\frac{n_e e^2}{m_e \epsilon_0}}, \quad (2)$$

where e and m_e are the electron charge and mass, and ϵ_0 is the permittivity of free space. Typical ionospheric plasma frequency values are of the order of a few MHz. The phase shift due to wave propagation is (thin-screen approximation)

$$\phi_{\text{tot}} = \int dz \frac{2\pi\eta(z)}{\lambda}, \quad (3)$$

where $\lambda = c/\nu$ is the electromagnetic wavelength (c is the speed of light in vacuum), and z is the distance along the propagating ray. Using equation 1, we get

$$\phi_{\text{tot}} = \int dz \frac{2\pi\nu}{c} - \frac{1}{2} \int dz \frac{2\pi\nu_p^2}{c\nu}, \quad (4)$$

where the second term is the additional phase shift introduced due to the plasma (ϕ say), and the first term (geometric delay) is usually absorbed into the interferometer measurement equation. It follows that the propagation phase ϕ is inversely proportional to the frequency ν :

$$\phi(\nu) \propto \nu^{-1}. \quad (5)$$

2.2 Spatial properties

Spatial variations in plasma density n_e may be modelled as a 3-dimensional Gaussian random field with a power spectrum given by a $-11/3$ index power-law corresponding to Kolmogorov-type turbulence⁴ (Wheelon 2001). Since $\nu_p \propto n_e^{1/2}$ (equation 2), and since $\phi \propto \nu_p^2$ (equation 5), it follows that $\phi \propto n_e$. Hence, the propagation phase is also a Gaussian random field with a power-spectrum given by

$$|\tilde{\phi}(k)|^2 \propto k^{-11/3} \quad k_o < k < k_i, \quad (6)$$

where k is the length of the spatial wave-number vector \mathbf{k} , and k_o is the wavenumber corresponding to the outer-scale or the energy-injection scale, and k_i corresponds to the inner-scale or energy dissipation scale. We will assert the thin-screen approximation by interpreting k as the length of the 2-dimensional (transverse coordinates) spatial wavenumber vector, since $k_z = 0$ essentially corresponds to the path integrated phase used in the thin-screen approximation. For $k < k_o$ the power spectrum is expected to be flat, and for $k > k_i$ the power spectrum is expected to fall off rapidly to zero. For the ionospheric case, the inner-scale is thought to be of the order of a few metres (ion-gyroradius) (Wheelon 2001). In the regime of interest to us, both the Fresnel scale (defined later) and baseline lengths are significantly larger than the inner-scale and its effects may be safely ignored. In any case, the steep $-11/3$ index power-law gives negligible power in turbulence on such small scales. The outer-scale on the other hand can be several tens to hundreds of kilometre. Such scales are typically within the projected field of view of current wide-field telescopes on the ionosphere and it is prudent to retain the effects of eddies on scales larger than the outer-scale in widefield speckle noise calculations. To make the computations analytically tractable, we will choose a form that has a graceful transition from the inertial $11/3$ -law range ($k > k_o$) and the flat range ($k < k_o$)⁵:

$$|\tilde{\phi}(k)|^2 = \frac{5\phi_0^2}{6\pi k_o^2} \left[\left(\frac{k}{k_o} \right)^2 + 1 \right]^{-11/6}, \quad (7)$$

where we have normalised the spectrum to represent a 2-dimensional Gaussian random field (phase screen) with variance ϕ_0^2 . We caution the reader that since there is no generally accepted theory of ionospheric plasma turbulence, neither the injection scale k_o , nor the index ($\beta = 11/3$ here) are uniquely determined. We have chosen the $11/3$ law since it corresponds to a well known Kolmogorov law, and since it falls within the range of $3 < \beta < 4$ suggested by measurements of ionospheric scintillation (Rufenach 1972). The two-dimensional Fourier transform of equation 7 gives the spatial auto-correlation function of the ionospheric phase:

$$\rho(r) = \frac{5}{3} \frac{(\pi k_o r)^{5/6}}{\Gamma(11/6)} K_{5/6}(2\pi k_o r), \quad (8)$$

where r is the spatial separation, $\Gamma(\cdot)$ is the Gamma function, and $K_{5/6}$ is the modified Bessel function of the second kind of order $\frac{5}{6}$. The auto-correlation function $\rho(r)$ has been normalised such that $\rho(0) = 1$. For spatial separations significantly smaller than the outer scale ($r k_o \ll 1$) we can use a small argument expansion of the Bessel function to get

$$\rho(r) \approx \left[1 - \frac{\Gamma(1/6)}{\Gamma(11/6)} (\pi k_o r)^{5/3} \right]. \quad (9)$$

The spatial correlation is often described in terms of the structure function which is easier to measure in practice:

$$\mathcal{D}(\mathbf{r}) = \langle (\phi(\mathbf{r}_0 + \mathbf{r}) - \phi(\mathbf{r}_0))^2 \rangle = 2\phi_0^2 [\rho(0) - \rho(r)]. \quad (10)$$

Using equation 9, we can show that the structure function takes the usual form for Kolmogorov turbulence:

$$\mathcal{D}(r) \approx \left(\frac{r}{r_d} \right)^{5/3}, \quad (11)$$

where the approximation holds for $\pi r k_o \ll 1$, and $\mathcal{D}(r) \lesssim 2\langle \phi^2 \rangle$, the latter being its asymptotic value, and r_d is the diffractive-scale: the separation at which the phase structure-function reaches unity. The diffractive scale is given by

$$r_d = \frac{1}{\pi k_o} \left(\frac{\Gamma(11/6)}{2\Gamma(1/6)\phi_0^2} \right)^{3/5}. \quad (12)$$

Finally, using the frequency scaling from equation 5, we can show that the diffractive scale varies with frequency as

$$r_d(\nu) \propto \nu^{6/5}. \quad (13)$$

⁴ The statistics of ionospheric phase solutions in LOFAR data also attest this assumption (Mevius et al. priv. comm.).

⁵ The choice of the power spectrum is similar to the one made by von Karman (1948) in his study of fluid-turbulence.

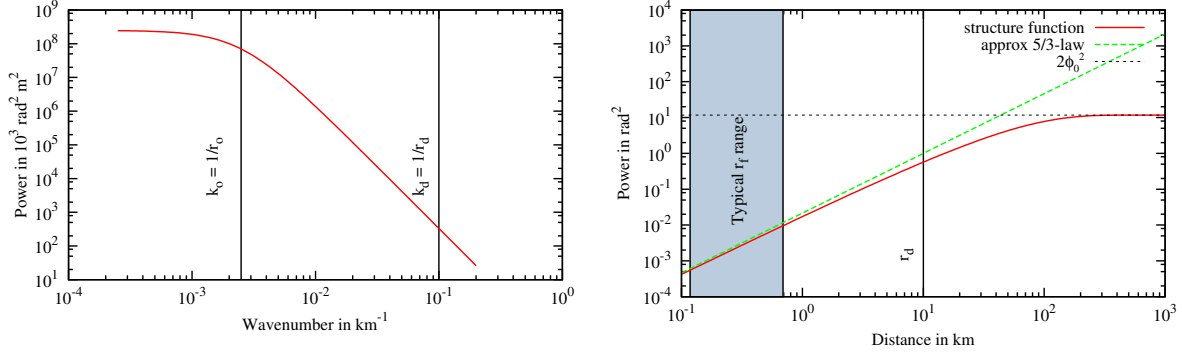


Figure 1. Phase power spectrum (left) and the corresponding structure function (right) with typical values for ionospheric turbulence parameters ($r_o = 400$ km, $r_d = 10$ km, $\phi_0^2 = 5.87 \text{ rad}^2$). The shaded region shows the range of Fresnel scale values (for an ionospheric height of 300 km) for frequencies between 30 MHz and 1 GHz. .

Typical values of the diffractive scale at 150 MHz vary between ~ 5 km to ~ 30 km (Mevius et al. priv. comm.). Any two of the three variables k_o , $\langle \phi^2 \rangle$, and r_d uniquely determine the power spectrum. Fig. 1 shows an example power spectrum and its structure function for typical ionospheric parameters (at 150 MHz) of $r_o = 400$ km, $r_d = 10$ km, $\phi_0^2 = 5.87 \text{ rad}^2$.

2.3 Time dependence

The temporal variation in interferometric phase is usually dominated by relative motion between the observer and the plasma irregularities rather than an intrinsic evolution of the turbulence itself. For instance, ionospheric turbulence is expected to ‘ride along’ a bulk wind at speeds of the order of $v = 100 - 500 \text{ km hr}^{-1}$. This couples the temporal and spatial correlation properties of ionospheric phase which we explore in Section 5. Regardless, spatial decorrelation of ionospheric on a scales of r implies a temporal decorrelation on a time scale of

$$\tau_d = r/v. \quad (14)$$

As shown in Section 5.1, the relevant spatial decorrelation scales is of the order of the baseline length with a minimum decorrelation scale equal to the Fresnel scale. For the case of ionospheric effects in current low-frequency arrays, the above spatial scales vary from few hundred metres to several tens of kilometres. Hence, the relevant temporal decorrelation scales are of the order of few seconds to several minutes.

3 SINGLE BASELINE STATISTICS

In this section we derive the statistical properties of the interferometric visibility for a given baseline (antenna pair). We will assume that all antennas of the interferometer lie on a plane that is parallel to the diffraction screen, and denote all positions as vectors in two-dimensions. The geometry is sketched in Fig. 2. The electric field on the observer plane due to a unit flux source at position-vector \mathbf{l} is given by the Kirchhoff-Fresnel integral (Born & Wolf 1999) evaluated on the diffraction plane (phase-screen in our case):

$$E(\mathbf{r}, \mathbf{l}) = \frac{1}{i\lambda h} \int d^2\mathbf{x} \exp \left[\frac{i\pi}{\lambda h} (\mathbf{x} - \mathbf{r})^2 \right] \exp [-i2\pi\mathbf{x} \cdot \mathbf{l}/\lambda] \exp [i\phi(\mathbf{x})], \quad (15)$$

where we have used the short-hand notation $\mathbf{x}^2 = |\mathbf{x}|^2$. The second exponent accounts for the geometric delay in arrival time of the wavefront on different points on the diffraction plane, and the third exponent denotes the phase modulation of the wavefront as it crosses the phase screen. The first exponent which we will call the ‘Fresnel exponential’, represents the effects of relative path-length differences between the ‘scatterers’ on the diffraction screen at \mathbf{x} and the observer at \mathbf{r} . Note that relative distance in equation 15 is only accurate to quadratic order (Fresnel diffraction). The higher order terms in the scatterer-observer distance become comparable to a wavelength if the FOV exceeds about 10 deg. By completing the square in the first two exponents, we get

$$E(\mathbf{r}, \mathbf{l}) = \frac{1}{i\lambda h} \exp [-i2\pi\mathbf{r} \cdot \mathbf{l}/\lambda] \exp [-i\pi h \mathbf{l}^2/\lambda] \int d^2\mathbf{x} \exp \left[\frac{i\pi}{\lambda h} (\mathbf{x} - \mathbf{r} - h\mathbf{l})^2 \right] \exp [i\phi(\mathbf{x})]. \quad (16)$$

Making a change of variable: $\mathbf{x} - \mathbf{r} - h\mathbf{l} \rightarrow \mathbf{x}$, we get

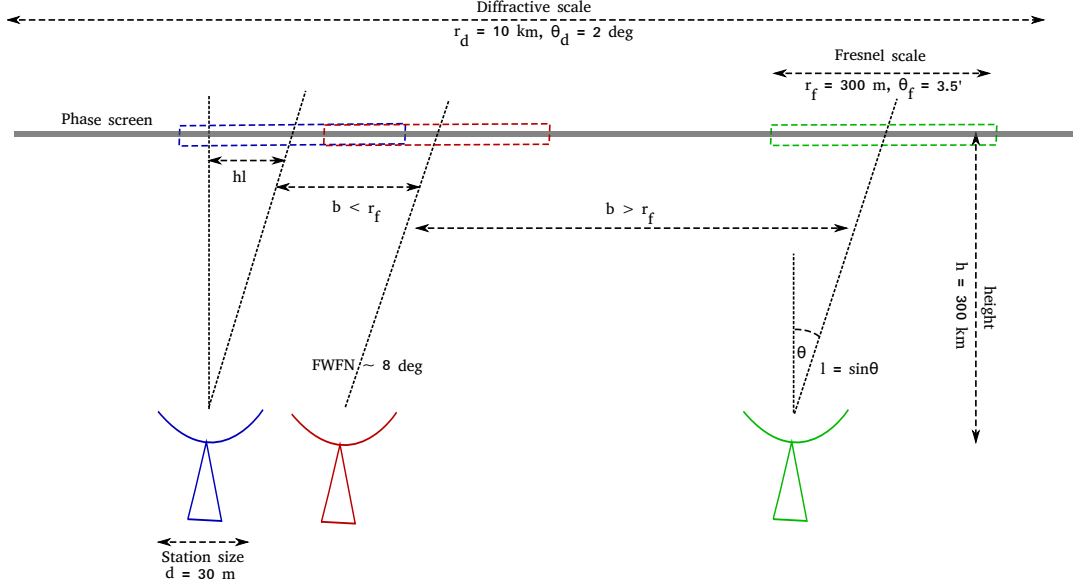


Figure 2. A not-to-scale sketch showing the assumed geometry in this paper along with some length- and angular-scales that are relevant for our discussion. The numerical values are typical for the case of ionospheric propagation at $\nu = 150$ MHz.

$$E(\mathbf{r}, \mathbf{l}) = \frac{1}{i\lambda h} \exp[-i2\pi \mathbf{r} \cdot \mathbf{l} / \lambda] \exp[-i\pi h \mathbf{l}^2 / \lambda] \int d^2 \mathbf{x} \exp\left[\frac{i\pi}{\lambda h} \mathbf{x}^2\right] \exp[i\phi(\mathbf{x} + \mathbf{r} + h\mathbf{l})], \quad (17)$$

which is basically a convolution of the phase modulating function with the Fresnel exponential. The complex Fresnel exponential varies rapidly for $\mathbf{x}^2 \gtrsim r_F$ where $r_F = \sqrt{\lambda h / (2\pi)}$ is called the Fresnel-scale (depicted as coloured boxes in Fig. 2). Consequently, most of the contribution to the integral comes from a small region of size r_F around the stationary-phase point $\mathbf{x} = \mathbf{0}$. If the phase variation $\phi(\mathbf{x})$ on the diffraction screen is small ($\ll 1$ radian) over spatial scales of the size of r_F , then the integral may be approximated by its value at the stationary-phase point. This is often referred to as the pierce-point approximation since we are reducing the electric-field phase in a certain direction \mathbf{l} to the ionospheric-phase at $\mathbf{r} + h\mathbf{l}$, which is the point of intersection of a ray travelling from \mathbf{r} in direction \mathbf{l} with the scattering screen:

$$E_{pp}(\mathbf{r}, \mathbf{l}) = \exp[-i2\pi \mathbf{r} \cdot \mathbf{l} / \lambda] \exp[-i\pi h \mathbf{l}^2 / \lambda] \exp[i\phi(\mathbf{r} + h\mathbf{l})], \quad (18)$$

where the subscript denotes the pierce-point approximation.

The visibility on a baseline \mathbf{b} due to a source at \mathbf{l} is defined as

$$V(\mathbf{b}, \mathbf{l}) \equiv E(\mathbf{r}, \mathbf{l}) E^*(\mathbf{r} + \mathbf{b}, \mathbf{l}), \quad (19)$$

where $(.)^*$ denotes complex conjugation. Since we assume the statistics of the ionospheric phase to be spatially invariant, the visibility statistics are independent of the choice of \mathbf{r} and we choose \mathbf{r} to be the origin. Using the expression for the electric field from equations 17 and 18, we can write the visibility for a unit flux-density source without and with the pierce-point approximation as

$$V(\mathbf{b}, \mathbf{l}) = \frac{\exp[i2\pi \mathbf{b} \cdot \mathbf{l} / \lambda]}{\lambda^2 h^2} \int \int d^2 \mathbf{x}_1 d^2 \mathbf{x}_2 \exp\left[\frac{i\pi}{\lambda h} (\mathbf{x}_1^2 - \mathbf{x}_2^2)\right] \exp[i(\phi(\mathbf{x}_1 + h\mathbf{l}) - \phi(\mathbf{x}_2 + h\mathbf{l} + \mathbf{b}))] \quad \text{and} \quad (20)$$

$$V_{pp}(\mathbf{b}, \mathbf{l}) = \exp[i2\pi \mathbf{b} \cdot \mathbf{l} / \lambda] [\exp[i(\phi(h\mathbf{l}) - \phi(h\mathbf{l} + \mathbf{b}))]], \quad \text{respectively.} \quad (21)$$

Due to the convolution with the Fresnel exponential, the pierce-point approximation is accurate only when $b \gtrsim r_F$ where the Fresnel-zones for the two receiving antennas do not overlap (see Fig. 2). In any case, the visibility from the entire sky can be written in terms of the point-source visibility as

$$V(\mathbf{b}) = \int \frac{d^2 \mathbf{l}}{\sqrt{1 - \mathbf{l}^2}} I(\mathbf{l}) V(\mathbf{b}, \mathbf{l}), \quad (22)$$

where $I(\mathbf{l})$ is the apparent-sky surface brightness as seen through the primary beam of the antennas comprising the interferometer elements (primary beam). We are primarily interested in the statistical properties of $V(\mathbf{b})$ such as its expectation $\langle V(\mathbf{b}) \rangle$, and variance $\sigma_V^2 = \langle |V(\mathbf{b})|^2 \rangle - |\langle V(\mathbf{b}) \rangle|^2$. We want to compute these statistics as ensembles over different ionospheric phase screen realisations. The reader should not confuse these expectations with the expectations over the inherent randomness in emission from astrophysical sources which has been made implicit in our notation. The expected value of the visibility is then given by

$$\langle V(\mathbf{b}) \rangle = \int \frac{d^2 \mathbf{l}}{\sqrt{1-l^2}} I(\mathbf{l}) \langle V(\mathbf{b}, \mathbf{l}) \rangle. \quad (23)$$

The above expectation is analytically tractable and yields (see Appendix A for proof)

$$\langle V(\mathbf{b}) \rangle = \langle V_{\text{pp}}(\mathbf{b}) \rangle = \int \frac{d^2 \mathbf{l}}{\sqrt{1-l^2}} I(\mathbf{l}) \exp[i2\pi \mathbf{b} \cdot \mathbf{l} / \lambda] \exp\left[-\frac{1}{2} \mathcal{D}(\mathbf{b})\right] = V(\mathbf{b}) \exp\left[-\frac{1}{2} \mathcal{D}(\mathbf{b})\right]. \quad (24)$$

Hence the expected visibility is equal to the visibility in the absence of the ionosphere, diminished by a factor that depends on the ionospheric phase structure function for a separation given by the baseline. Note that the above equation (second-moment of the electric field) is independent of the strength of scattering, and identical for both cases (with and without the pierce-point approximation). As we will soon see, this similarity does not extend to higher moments of the electric field.

The visibility variance due to the entire sky is given by

$$\sigma^2[V(\mathbf{b})] = \int \frac{d^2 \mathbf{l}_a}{\sqrt{1-l_a^2}} I(\mathbf{l}_a) \int \frac{d^2 \mathbf{l}_b}{\sqrt{1-l_b^2}} I(\mathbf{l}_b) \sigma^2[V(\mathbf{b}, \mathbf{l}_a, \mathbf{l}_b)]. \quad (25)$$

Analytically computing the two-source visibility variance ($\sigma^2[V(\mathbf{b}, \mathbf{l}_a, \mathbf{l}_b)]$) is tedious and not very enlightening. The interested reader may find the proof in Appendix B, and we present the final expressions here:

$$\sigma^2[V_{\text{pp}}(\mathbf{b}, \mathbf{l}_a, \mathbf{l}_b)] = 4 \exp[i2\pi \mathbf{b} \cdot \Delta \mathbf{l} / \lambda] \int d^2 \mathbf{q} \exp[-i2\pi h \mathbf{q} \cdot \Delta \mathbf{l}] \left| \tilde{\phi}(\mathbf{q}) \right|^2 \sin^2(\pi \mathbf{q} \cdot \mathbf{b}), \text{ where } \Delta \mathbf{l} = \mathbf{l}_a - \mathbf{l}_b, \quad (26)$$

for the pierce-point approximation, and

$$\sigma^2[V(\mathbf{b}, \mathbf{l}_a, \mathbf{l}_b)] = 4 \exp[i2\pi \mathbf{b} \cdot \Delta \mathbf{l} / \lambda] \int d^2 \mathbf{q} \exp[-i2\pi h \mathbf{q} \cdot \Delta \mathbf{l}] \left| \tilde{\phi}(\mathbf{q}) \right|^2 \sin^2(-\pi \mathbf{q} \cdot \mathbf{b} + \pi \lambda h \mathbf{q}^2), \quad (27)$$

for the full Kirchhoff-Fresnel integral. In deriving the above, we have assumed that the scattering is weak: the phase fluctuations within a Fresnel-scale are small. The visibility variance is expressed as an integral of various wavemodes \mathbf{q} in the phase power-spectrum that are modulated by a sine-squared term which is a consequence of the Fresnel exponent. For this reason, this term is often called the Fresnel-filter (Cronyn 1972). In Section 3.1, the Fourier-domain representation will also be instrumental in developing a deeper intuitive understanding of Fresnel-diffraction by a phase modulating screen. The pierce-point expression is a special case of the full Kirchhoff-Fresnel evaluation where the Fresnel-scale in the Fresnel-filter goes to zero—a direct consequence of the stationary phase approximation.

Cronyn (1972) has derived an expression for visibility co-variance between two redundant baselines that are spatially displaced by \mathbf{d} and are looking at a single point-source. Whereas we are dealing with visibility co-variance between two sources separated by $\Delta \mathbf{l}$, his expression is identical to our equation 26 if we replace $h\Delta \mathbf{l}$ with \mathbf{d} . The similarity comes from the fact that both derivations are essentially evaluating the 4-point correlation of ionospheric phase (with the Fresnel convolution). In one case the 4-points are the pierce-points of the 4 antennas forming the redundant baseline pair, each looking in some direction. In the other case, the pierce-points are those of the two antennas forming the baseline, looking in two different directions.

The visibility variance due to the entire sky can now be written as

$$\sigma^2[V(\mathbf{b})] = 4 \int \frac{d^2 \mathbf{l}_a}{\sqrt{1-l_a^2}} I(\mathbf{l}_a) \int \frac{d^2 \mathbf{l}_b}{\sqrt{1-l_b^2}} I(\mathbf{l}_b) \exp[i2\pi \mathbf{b} \cdot \Delta \mathbf{l} / \lambda] \int d^2 \mathbf{q} \exp[-i2\pi h \mathbf{q} \cdot \Delta \mathbf{l}] \left| \tilde{\phi}(\mathbf{q}) \right|^2 \sin^2(-\pi \mathbf{q} \cdot \mathbf{b} + \pi \lambda h \mathbf{q}^2). \quad (28)$$

Interchanging the order of integration, we get

$$\sigma^2[V(\mathbf{b})] = 4 \int d^2 \mathbf{q} \left| \tilde{\phi}(\mathbf{q}) \right|^2 \sin^2(-\pi \mathbf{q} \cdot \mathbf{b} + \pi \lambda h \mathbf{q}^2) \int \frac{d^2 \mathbf{l}_a}{\sqrt{1-l_a^2}} I(\mathbf{l}_a) \int \frac{d^2 \mathbf{l}_b}{\sqrt{1-l_b^2}} I(\mathbf{l}_b) \exp[i2\pi(\mathbf{b} - \lambda h \mathbf{q}) \cdot \Delta \mathbf{l} / \lambda]. \quad (29)$$

The integrations with \mathbf{l}_a and \mathbf{l}_b yield the sky power-spectrum computed at $\mathbf{b} - \lambda h \mathbf{q}$:

$$\int \frac{d^2 \mathbf{l}_a}{\sqrt{1-l_a^2}} I(\mathbf{l}_a) \int \frac{d^2 \mathbf{l}_b}{\sqrt{1-l_b^2}} I(\mathbf{l}_b) \exp[i2\pi(\mathbf{b} - \lambda h \mathbf{q}) \cdot \Delta \mathbf{l} / \lambda] = |V(\mathbf{b} - \lambda h \mathbf{q})|^2. \quad (30)$$

Hence the visibility variance for the Kirchhoff-Fresnel evaluation is

$$\sigma^2[V(\mathbf{b})] = 4 \int d^2 \mathbf{q} \left| \tilde{\phi}(\mathbf{q}) \right|^2 \sin^2(-\pi \mathbf{q} \cdot \mathbf{b} + \pi \lambda h \mathbf{q}^2) |V(\mathbf{b} - \lambda h \mathbf{q})|^2, \quad (31)$$

whereas the visibility variance for the pierce-point approximation is

$$\sigma^2[V_{\text{pp}}(\mathbf{b})] = 4 \int d^2 \mathbf{q} \left| \tilde{\phi}(\mathbf{q}) \right|^2 \sin^2(\pi \mathbf{q} \cdot \mathbf{b}) |V(\mathbf{b} - \lambda h \mathbf{q})|^2. \quad (32)$$

We have thus related the visibility variance to the statistics of ionospheric turbulence (via $|\tilde{\phi}(\mathbf{q})|^2$), the scattering geometry (via the Fresnel filter) and the sky power spectrum.

The pierce-point approximation leads to evident inconsistencies. For instance, when $\mathbf{b} = \lambda h \mathbf{q}$, the visibility variance receives contribution from the total power emission (diffuse) in the sky. In the Kirchhoff-Fresnel expression, however, the Fresnel filter vanishes for $\mathbf{b} = \lambda h \mathbf{q}$. However for $|\mathbf{b}| \gg r_F$, the Fresnel-filter term in equation 31 reduces to the one in equation 32. The pierce-point approximation works well for baselines far larger than the Fresnel-scale, but give erroneous results for baselines of the order of the Fresnel scale— an important conclusion for current and future low-frequency radio telescopes that have compact array configurations.

3.1 Physical interpretation in one-dimension

We will now present some physical intuition behind equation 31. In doing so our emphasis will be on the ‘meaning’ or significance of the terms and not on the algebraic correctness. Hence, we will simply use a 1-dimensional sky and phase-screen. Equation 31 is an integral on various Fourier modes (with spatial frequency q) of the modulating phase on the diffraction screen. The diffraction pattern on the observer plane is a superposition of the Fresnel diffraction patterns due to each of these Fourier modes. The amplitudes of these Fourier modes are mutually independent: $\langle \tilde{\phi}(q_1) \tilde{\phi}^*(q_2) \rangle = 0$ for $|q_1| \neq |q_2|$, and we can add the visibility variances due to individual Fourier modes as in equation 31. The electric field at position r on the observer plane $E(R)$ can be written in terms of the electric field on the diffraction plane $E_D(r)$ using the Fresnel-Kirchhoff integral:

$$E(R) = \frac{1}{\sqrt{i\lambda h}} \int dr E_D(r) \exp \left[\frac{i\pi}{\lambda h} (r - R)^2 \right] \exp [i\phi(r)]. \quad (33)$$

We will again make the weak scattering approximation and Taylor expand the exponent containing the modulation phase $\phi(r)$ to write

$$E(R) = \frac{1}{\sqrt{i\lambda h}} \int dr E_D(r) \exp \left[\frac{i\pi}{\lambda h} (r - R)^2 \right] + \frac{i}{\sqrt{i\lambda h}} \int dr E_D(r) \phi(r) \exp \left[\frac{i\pi}{\lambda h} (r - R)^2 \right]. \quad (34)$$

The first integral gives the electric field on the observer plane in the absence of any scattering, say $E_o(R)$. The second term is the scattered field $E_s(R)$, and it is the interference between these two fields that we are interested in. $E_s(R)$ can be written by expressing $\phi(r)$ as a Fourier transform as

$$E(R) = E_o(R) + \frac{i}{\sqrt{i\lambda h}} \int dq \tilde{\phi}(q) \int dr E_D(r) \exp \left[\frac{i\pi}{\lambda h} (r - R)^2 \right] \exp [i2\pi q r]. \quad (35)$$

Completing the square in the complex exponent, we get

$$E(R) = E_o(R) + \frac{i}{\sqrt{i\lambda h}} \int dq \tilde{\phi}(q) \exp [i2\pi q R] \exp [-i\pi \lambda h q^2] \int dr E_D(r) \exp \left[\frac{i\pi}{\lambda h} (r - R + \lambda h q)^2 \right]. \quad (36)$$

The integral is equal to the incident field shifted by $\lambda h q$: $E_o(R - \lambda h q)$. Hence, we get

$$E(R) = E_o(R) + i \int dq E_o(R - \lambda h q) \tilde{\phi}(q) \exp [i2\pi q R] \exp [-i\pi \lambda h q^2]. \quad (37)$$

The lateral shift of the scattered field on the observer plane is a direct consequence of (weak) phase modulation of the electric field on the diffraction plane by a ‘phase-wave’ with spatial frequency of q . For instance, consider a plane wave travelling in direction l . Its geometric phase on the diffraction screen at position r is $2\pi l r$. Phase modulation by a ‘phase-wave’ of spatial frequency q adds an additional phase of $2\pi q r$. The aggregate phase is then $2\pi(l + q)r$ — that of a plane wave travelling in direction $l + q$. Hence, an incident wave from direction l emerges from the diffraction plane travelling in direction $l + q$. This is depicted in Fig. 3 where the sky is shown as a set of point sources (blue dots) on an imaginary ‘sky surface’. In the absence of the diffracting screen, the waves from these sources interfere to produce an instantaneous electric field on the observer’s plane $E_o(R)$ depicted as a stochastic blue curve. The diffracted waves, each being ‘deflected’ by an angle q form an interference pattern that is shifted on the observer’s plane by an amount $\lambda h q$. This is depicted as the stochastic red curve in Fig. 3. It is the interference between the direct incident field $E_o(R)$ and the stochastic⁶ scattered field $E_o(R - \lambda h q)$ that leads to most of the visibility scintillation or speckle noise. Due to a lateral shift of $\lambda h q$ between the interfering electric fields, visibility scintillation on a baseline b is indeed sensitive to sky structures on baseline $b - \lambda h q$ as evidenced in equation 31. Finally, the additional geometric phase terms in equation 37, are a consequence of the additional path-length travelled by the deflected

⁶ Stochastic here refers to the random nature of $\tilde{\phi}(q)$.

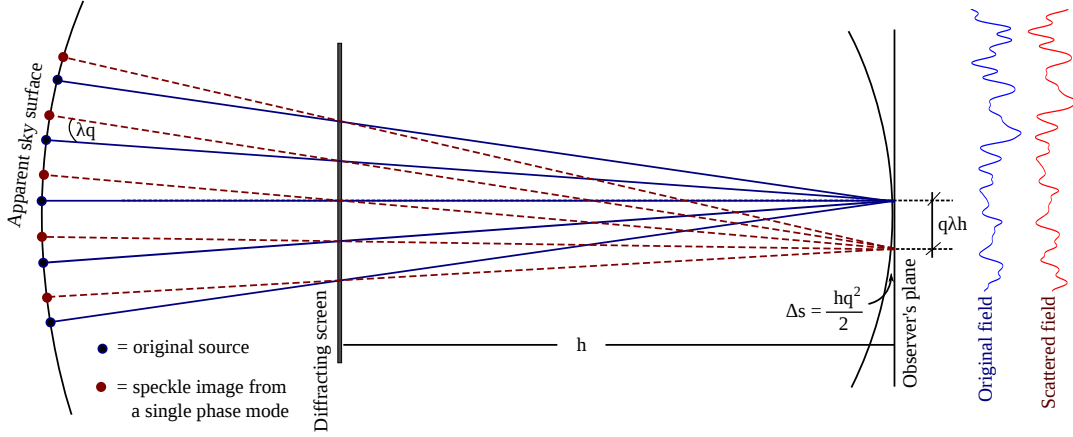


Figure 3. Cartoon (not actual ray-tracing) depicting the physical interpretation of equation 31. A single ionospheric phase mode with spatial frequency \mathbf{q} results in the displacement of the visibility on the observer plane by an amount $\mathbf{q}\lambda h$. Equivalently, part of the flux in a source in the direction \mathbf{l} is scattered into directions $\mathbf{l} + \mathbf{q}$ and $\mathbf{l} - \mathbf{q}$.

rays (including wavefront curvature effects), and lead to the sine-squared term (Fresnel filter) in equation 31.

We will demonstrate the above deductions more formally by considering a single wave mode: $\tilde{\phi}(\mathbf{q}) = \tilde{\phi}(\mathbf{q}_0)\delta(\mathbf{q}-\mathbf{q}_0) + \tilde{\phi}^*(\mathbf{q}_0)\delta(\mathbf{q}+\mathbf{q}_0)$, where $q_0 > 0$ and we have imposed conjugate symmetry to get a real phase field $\phi(r)$. The electric field on the observer's plane is then

$$E(R) = E_o(R) + i\tilde{\phi}(\mathbf{q}_0)E_o(R - \lambda h\mathbf{q}_0) \exp[i2\pi\mathbf{q}_0 R] \exp[-i\pi\lambda h\mathbf{q}_0^2] + i\tilde{\phi}^*(\mathbf{q}_0)E_o(R + \lambda h\mathbf{q}_0) \exp[-i2\pi\mathbf{q}_0 R] \exp[-i\pi\lambda h\mathbf{q}_0^2]. \quad (38)$$

The instantaneous visibility on baseline b can be written as

$$V(b) = E(-b/2)E^*(b/2) = V_o(b) + 2\tilde{\phi}^*(\mathbf{q}_0)V_o(b - \lambda h\mathbf{q}_0) \sin(-\pi\mathbf{q}_0 b + \pi\lambda h\mathbf{q}_0^2) + 2\tilde{\phi}(\mathbf{q}_0)V_o(b + \lambda h\mathbf{q}_0) \sin(\pi\mathbf{q}_0 b + \pi\lambda h\mathbf{q}_0^2), \quad (39)$$

where we have disregarded the higher order terms in $\tilde{\phi}(\mathbf{q}_0)$ which can be shown to reduce to zero up to fourth-order in the visibility variance. The fourth-order terms are expected to be negligible for weak scattering. The first terms $V_o(b)$ is the incident visibility in the absence of scattering, and the other terms are the result of interference between the incident and scattered fields. The variance of the visibility (over phase-screen realisations) may be computed by observing that $\langle [\tilde{\phi}(\mathbf{q}_0)]^n \rangle = \langle [\tilde{\phi}^*(\mathbf{q}_0)]^n \rangle = 0$, for $n = 1, 2$ and $\langle \tilde{\phi}(\mathbf{q}_0)\tilde{\phi}^*(\mathbf{q}_0) \rangle = |\tilde{\phi}(\mathbf{q}_0)|^2$:

$$\sigma^2[V(b)] = \sigma^2[V_o(b)] + 4|\tilde{\phi}(\mathbf{q}_0)|^2 \sin^2[-\pi\mathbf{q}_0 b + \pi\lambda h\mathbf{q}_0^2] |V_o(b - \lambda h\mathbf{q}_0)|^2 + 4|\tilde{\phi}(\mathbf{q}_0)|^2 \sin^2[\pi\mathbf{q}_0 b + \pi\lambda h\mathbf{q}_0^2] |V_o(b + \lambda h\mathbf{q}_0)|^2 \quad (40)$$

where $q_0 > 0$. The term $\sigma^2[V_o(b)]$ is the visibility noise in the absence of scattering (sky noise + receiver noise), and the second term is the speckle-noise contribution to the visibility variance. Since the complex amplitude for different wave-modes $\tilde{\phi}(\mathbf{q})$ are uncorrelated, we can express the visibility variance as an integral over variance due to a single wave mode as computed in equation 40:

$$\sigma^2[V(b)] = 4 \int_{q=-\infty}^{q=+\infty} dq |\tilde{\phi}(\mathbf{q})|^2 \sin^2(-\pi\mathbf{q}b + \pi\lambda h\mathbf{q}^2) |V_o(b - \lambda h\mathbf{q})|^2 \quad (\text{speckle noise component}) \quad (41)$$

where we have extended the limits of integration to include negative values of q . Equation 41 is a one-dimensional analogue of equation 31, but we derived it along with some physical intuition behind the nature of visibility scintillation. An ionospheric wave-mode of spatial-frequency q_0 creates a speckle which is a coherent copy of the original sky but shifted by an angle q_0 . The phase-coherence between the original sky sources and their respective (shifted) speckles leads to constructive and destructive interference on the observer plane. The interference pattern varies due to fluctuations in the plasma-screen (due to turbulence), leading to speckle-noise or equivalently visibility-scintillation. The reader may note that this interference-effect does not directly follow from application of the van Cittert-Zernike theorem often used in Fourier synthesis imaging, since it assumes that all sources are incoherent (or independent) radiators.

4 SPECKLE NOISE FOR A REALISTIC SKY MODEL

As shown in equation 31, to compute the speckle noise in visibilities, we need to know the sky power spectrum $|V(\mathbf{b})|^2$. The sky power-spectrum obviously depends on the part of the sky being observed. However, we expected it to have certain average

properties. On short baselines (large angular modes) the sky power spectrum is dominated by Galactic diffuse emission, and on longer baselines (small angular modes) the power spectrum is dominated by the contribution from a multitude of compact and point-like sources. Since the Fresnel filter vanishes for $\mathbf{b} \approx \lambda \mathbf{h} \mathbf{q}$, we expect a sub-dominant contribution from the Galactic diffuse emission, and in this section, we numerically compute the speckle noise due to point sources as a function of frequency and baseline length.

The sky power spectrum due to point sources can be written as

$$|V(\mathbf{b})|^2 = \sum_{a=0}^{N-1} \sum_{b=0}^{N-1} S_a S_b \exp [i2\pi \mathbf{b} \cdot (\mathbf{l}_a - \mathbf{l}_b)/\lambda], \quad (42)$$

where we have assumed the sky to consist of N sources, and the i^{th} source has a flux-density S_i . Clearly, the sky power spectrum depends on the angular distribution of sources and their relative flux-densities. For simplicity, we will assume that sources are distributed uniformly in the sky (no clustering). We will also assume that the averaged separation between sources $\mathbf{l}_a - \mathbf{l}_b$ is larger than the interferometer fringe spacing λ/b . In practice, this assumption implies that we count all sources within the interferometer fringe-spacing as a single point source. Under these assumptions, if there are many sources within each flux-density bin, then the complex exponential in equation 42 decorrelates the summations unless $a = b$. For $a = b$, we get

$$|V(\mathbf{b})|^2 = \sum_{a=0}^{N-1} S_a^2. \quad (43)$$

Hence, the speckle noise due to many point sources is equal to the speckle from a single point source with flux

$$S_{\text{eff}} = \sqrt{\sum_{a=0}^{N-1} S_a^2}. \quad (44)$$

We note here that the above assumptions give a baseline independent power spectrum which is sometimes referred to as the ‘Poisson-floor’ in the sky power spectrum due to point sources. A few dominant sources in the field will lead to an interference pattern which may deviate significantly from this Poisson-floor. However, bright sources present a large signal to noise ratio to solve for (self-calibration) the propagation phase within speckle-decorrelation frequency- and time-scales, and hence, we do not compute their speckle noise contributions assuming that they have been largely calibrated and removed. It is the speckle noise from the myriad of intermediate and low flux-density sources which may not be removed from direction dependent calibration due to insufficient signal to noise ratio that we are concerned with. S_{eff} can be evaluated using the density function for sources within different flux-bins:

$$\frac{d^2 N(S_t)}{dS_t d\Omega} = C S_t^{-\alpha} \nu^{-\beta} \text{ Jy}^{-1} \text{ sr}^{-1}, \quad (45)$$

where dN is the expected number of sources at frequency ν per unit solid angle whose flux lie within an interval dS_t about S_t , C is a normalising constant (defined later), and α and β are typically negative and depend on the flux range. Note that the above source count is defined for the true flux, not apparent flux. The apparent flux at position \mathbf{l} on the sky is given by

$$S(\mathbf{l}) = S_t B(\mathbf{l}, \nu), \quad (46)$$

where $B(\mathbf{l}, \nu)$ is the primary beam factor at frequency ν in direction \mathbf{l} . For our speckle noise calculations, we are interested in the source counts for the primary-beam weighted sky $N(S)$ which is the number of sources in the visible sky whose apparent flux-densities lie in an interval dS about S . Integrating over the visible 2π solid angle, we can write

$$\frac{dN(S)}{dS} = \int \int_{2\pi} d\Omega \frac{d^2 N(S/B(\mathbf{l}, \nu))}{dS_t d\Omega} \left| \frac{dS_t}{dS} \right|, \quad (47)$$

where, we have made a change of variables from S_t to S , with a simple scaling by the Jacobian. We can do this since the relationship between true and apparent flux is monotonic. Using the source-counts from equation 45, we get

$$\frac{dN(S)}{dS} = C S^{-\alpha} \nu^{-\beta} \int \int_{2\pi} d\Omega B^{\alpha-1}(\mathbf{l}, \nu). \quad (48)$$

We can then define an effective beam as⁷

$$B_{\text{eff}}(\nu) = \int \int_{2\pi} d\Omega B^{\alpha-1}(\mathbf{l}, \nu), \quad (49)$$

and write the number of sources in the visible sky with apparent flux between S and $S + dS$ as

⁷ For $\alpha = 2.5$ (typical value) the effective beam B_{eff} is about 20 – 25% lower than the area under the beam.

$$\frac{dN(S)}{dS} = CB_{\text{eff}}(\nu)S^{-\alpha}\nu^{-\beta}. \quad (50)$$

We can now evaluate the relevant quantity $S_{\text{eff}} = \sqrt{\sum S^2}$ using the source counts as

$$\begin{aligned} S_{\text{eff}}^2 &= \int_{S_{\text{min}}}^{S_{\text{max}}} dS \frac{dN(S)}{dS} S^2 \\ &= \frac{CB_{\text{eff}}(\nu)\nu^{-\beta}}{3-\alpha} (S_{\text{max}}^{3-\alpha} - S_{\text{min}}^{3-\alpha}) \approx \frac{CB_{\text{eff}}(\nu)\nu^{-\beta}}{3-\alpha} S_{\text{max}}^{3-\alpha}, \end{aligned} \quad (51)$$

where the approximation holds since $\alpha < 3$ (typically). This implies that most of the speckle noise contribution comes from bright sources. It is then relevant to evaluate to what flux limit self-calibration is able to remove phase effects on the brightest sources. This limit is array and field dependent, a detailed discussion of which is beyond the scope of this paper. We will however continue our discussion by using numbers that are representative for current arrays at 150 MHz. As will be shown in Sec. 5, the ionospheric phase decorrelates on time-scales of a few seconds on baselines of the order of the Fresnel scale (100s of metres). Conservatively assuming a system equivalent flux density of 3000 Jy (for a 30 metre aperture), the thermal noise per visibility for a 2 sec, 1 MHz integration is about 1.5 Jy. We will assume that ionospheric phase effects on all sources above 7.5 Jy (SNR of 5 per visibility) are perfectly removed: $S_{\text{max}}(150 \text{ MHz}) = 7.5 \text{ Jy}$. A 7.5 Jy source at 150 MHz corresponds to a flux density of about 1.5 Jy at 1.4 GHz. Based on the 1.4 GHz source counts of Windhorst et al. (1985) (their Fig. 4a) we will use

$$\frac{dN(S)}{dS} = 3 \times 10^3 \left(\frac{B_{\text{eff}}(\nu)}{1 \text{ sr}} \right) \left(\frac{S}{1 \text{ Jy}} \right)^{-\alpha} \left(\frac{\nu}{150 \text{ MHz}} \right)^{-\beta} \quad \text{with } \alpha = 2.5, \beta = 0.7. \quad (52)$$

For a 30 metre diameter aperture we numerically compute $B_{\text{eff}}(150 \text{ MHz}) = 0.0042 \text{ sr}$, using which we get $S_{\text{eff}}(150 \text{ MHz}) \approx 8.5 \text{ Jy}$. We can then scale the effective flux to other frequencies using

$$S_{\text{eff}}^2(\nu) = 8.5^2 \frac{B_{\text{eff}}(\nu)}{B_{\text{eff}}(150 \text{ MHz})} \left(\frac{\nu}{150 \text{ MHz}} \right)^{-0.7} \left(\frac{S_{\text{max}}(\nu)}{S_{\text{max}}(150 \text{ MHz})} \right)^{0.5} \text{ Jy}. \quad (53)$$

For simplicity, we will assume that $S_{\text{max}}(\nu)$ linearly depends on the system equivalent flux density, which itself scales with frequency as $\nu^{-2.5}$. Additionally, the ratio of effective beam area can be replaced by the area under the beam itself. Numerical evaluation of beam area shows that the error we make in the ratio is below a few percent. Since the area under the beam scales as $(d\nu)^{-2}$, where d is the diameter of the receiving aperture (antenna) we can write the final scaling law as

$$S_{\text{eff}}(\nu) \approx 8.5 \left(\frac{d}{30 \text{ metre}} \right)^{-1} \left(\frac{\nu}{150 \text{ MHz}} \right)^{-1.975} \text{ Jy}. \quad (54)$$

Fig. 4 shows some speckle noise rms estimates as a function of baseline length for $S_{\text{eff}} = 8.5 \text{ Jy}$ (at 150 MHz), and $d = 30 \text{ metre}$. The four panels are for different frequencies between 50 and 200 MHz, and the different solid lines show the speckle noise for a range of ionospheric diffractive scales (specified at 150 MHz) typical to the LOFAR site (Mevius et al. priv. comm.) situated at mid-latitudes. The dashed lines show the speckle-noise computed using the pierce-point approximation, which as discussed before, gives inaccurate results at baselines $\lesssim r_F$. Also shown in the figure are the thermal noise (sky noise only) for a 30 metre primary aperture, assuming an integration bandwidth of 1 MHz, and integration time corresponding to the speckle-noise decorrelation time-scale for each baseline (computed in Section 5.1). Since $S_{\text{eff}}(\nu)$ and the thermal noise do not scale with highly disparate indices (-1.975 and 2.5 respectively), we expect the majority of spectral variation in thermal to speckle-noise ratio to be a result of increasing scattering strength with decreasing frequency.

The speckle noise values in Fig. 4 are computed assuming perfect removal (using direction dependent calibration) of speckle-noise from all sources brighter than $S_{\text{max}}(\nu) = 7.5(\nu/150 \text{ MHz})^{-2.5} \text{ Jy}$. Since speckle-noise is dominated by the brighter sources in the field, the reader should interpret Fig. 4 as an optimistic scenario. A final comment concerns the benefits of solving for ionospheric phases (within decorrelation time) for the most luminous sources in the source subtraction step. For the above parameters, $\sim 50\%$ of the speckle noise rms comes from the first 10 brightest sources and $\sim 90\%$ comes from the first 250 brightest sources.

5 COHERENCE PROPERTIES OF SPECKLE NOISE

So far, we have derived the statistical properties of visibility scintillation due to propagation through a turbulent plasma. These statistics must be interpreted as those for the case of infinitesimal bandwidth and integration time (quasi-monochromatic snapshot visibilities). In reality visibilities are always measured with certain spatial, temporal, and spectral averaging. Additionally, aperture synthesis results in averaging of visibilities on all the above dimensions. Accounting for these averaging effects requires knowledge of coherence properties of visibility scintillation in all three dimensions.

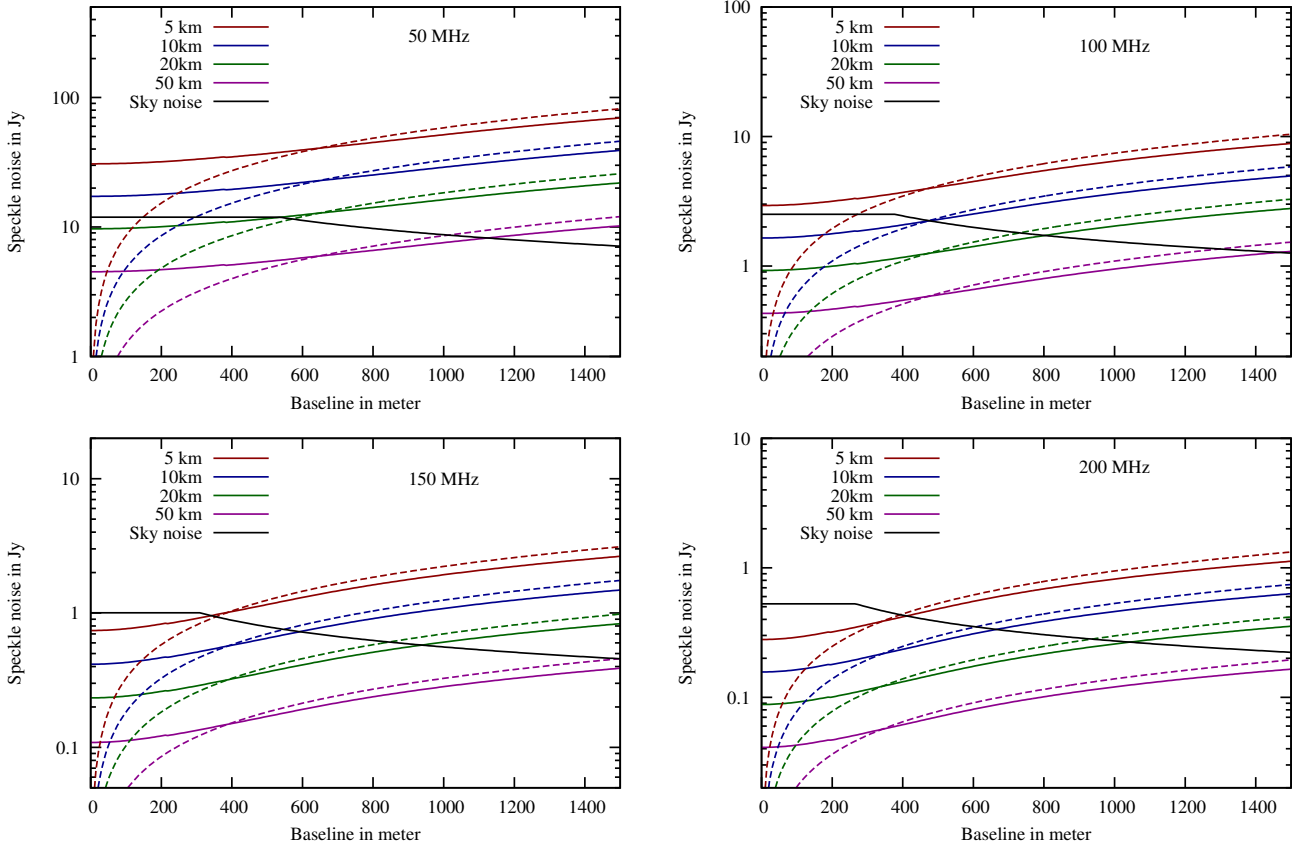


Figure 4. Speckle noise rms (optimistic scenario) per snapshot visibility for different ionospheric diffractive scales (specified at 150 MHz), for a realistic source distribution and a primary aperture diameter of 30 metre. The two sets of curves (dashed and solid) are for the pierce-point approximation and the full Kirchhoff-Fresnel solution respectively. The different panels are for different frequencies (50, 100, 150, and 200 MHz). Also shown for comparison (solid black) is the sky noise in visibilities assuming an integration over of 1 MHz in frequency and the speckle-noise decorrelation time-scale.

5.1 Temporal coherence

Temporal decorrelation of phase is expected to be mainly driven by bulk-motion of plasma turbulence relative to the observer, rather than the evolution of the turbulence itself. The visibility at time t can be written as (making the time argument explicit):

$$V(\mathbf{b}, \mathbf{l}, t) = \frac{\exp[i2\pi\mathbf{b} \cdot \mathbf{l}/\lambda]}{\lambda^2 h^2} \int \int d^2\mathbf{x}_1 d^2\mathbf{x}_2 \exp\left[\frac{i\pi}{\lambda h}(\mathbf{x}_1^2 - \mathbf{x}_2^2)\right] \exp[i(\phi(\mathbf{x}_1 + h\mathbf{l} + \mathbf{v}t) - \phi(\mathbf{x}_2 + h\mathbf{l} + \mathbf{b} + \mathbf{v}t))] \quad (55)$$

where the vector \mathbf{v} is the bulk wind velocity with which the ‘frozen’ plasma irregularities move, and we have neglected the effects of varying baseline projection due to Earth rotation. The two-source visibility coherence on a temporal separation of τ is then

$$\sigma_\tau^2[V(\mathbf{b}, \mathbf{l}_a, \mathbf{l}_b, \tau)] = \langle V(\mathbf{b}, \mathbf{l}_a, t=0) V^*(\mathbf{b}, \mathbf{l}_b, t=\tau) \rangle \quad (56)$$

The derivation for the above temporal covariance follows the same steps as the one in Appendix B with $h\Delta\mathbf{l}$ replaced by $h\Delta\mathbf{l} + \mathbf{v}\tau$. Hence, we can write

$$\sigma_\tau^2[V(\mathbf{b}, \mathbf{l}_a, \mathbf{l}_b, \tau)] = 4 \int d^2\mathbf{q} \exp[-i2\pi(h\mathbf{q} \cdot \Delta\mathbf{l} + \mathbf{q} \cdot \mathbf{v}\tau)] \left| \tilde{\phi}(\mathbf{q}) \right|^2 \sin^2(-\pi\mathbf{q} \cdot \mathbf{b} + \pi\lambda h\mathbf{q}^2) \quad (57)$$

The visibility variance due to the entire sky can now be written as (similar to equation 31)

$$\sigma_\tau^2[V(\mathbf{b}, \tau)] = 4 \int d^2\mathbf{q} \left| \tilde{\phi}(\mathbf{q}) \right|^2 \sin^2(-\pi\mathbf{q} \cdot \mathbf{b} + \pi\lambda h\mathbf{q}^2) |V(\mathbf{b} - \lambda h\mathbf{q})|^2 \exp[-i2\pi\mathbf{q} \cdot \mathbf{v}\tau] \quad (58)$$

which is basically a Fourier transform relationship with \mathbf{q} and $\mathbf{v}\tau$ as Fourier-conjugates. This makes sense, since a lateral displacement of plasma wave-modes by an amount $\mathbf{v}\tau$ decorrelates their aggregate phase over a ‘bandwidth’ of $\Delta q = 1/(\mathbf{v}\tau)$. The temporal decorrelation characteristics for the point source contribution to visibilities is given by replacing $|V(\mathbf{x})|^2$ in

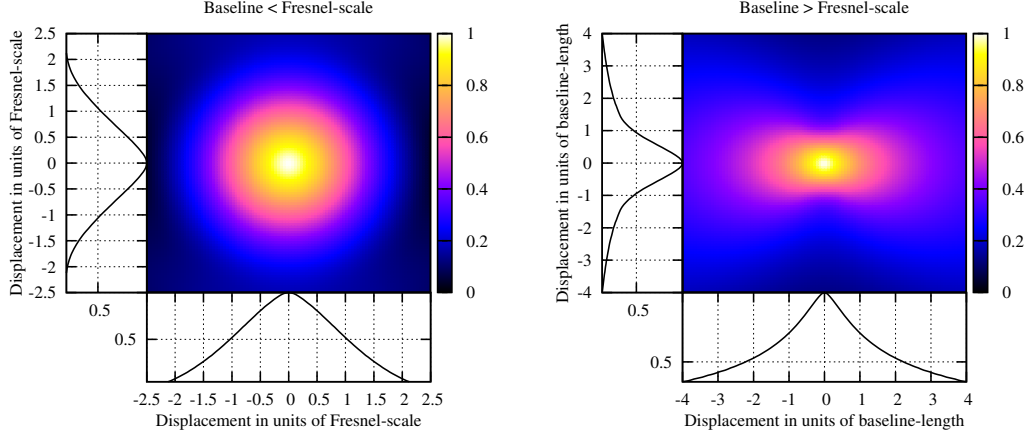


Figure 5. Plot showing the correlation properties of speckle noise from point-like sources as a function of displacement along (horizontal axis) and perpendicular (vertical axis) to the interferometer baseline. Displacement can be due to bulk motion of plasma-turbulence, or lateral shift of the baseline vector. Left and right panels show the correlation when the interferometer-baseline is smaller than or larger than the Fresnel-scale respectively.

equation 58 by S_{eff}^2 . The resulting integration can be done numerically, and we show the results⁸ in Fig. 5 for two limiting cases: (i) $|\mathbf{b}| \lesssim r_F$ where the $\pi\lambda h \mathbf{q}^2$ term in the argument of the sine-squared function dominates, and (ii) $|\mathbf{b}| \gtrsim r_F$ where the $\pi \mathbf{q} \mathbf{b}$ term dominates. In the second case, the Fourier transform can also be carried out analytically to yield

$$\sigma_\tau^2[V(\mathbf{b})] \approx S_{\text{eff}}^2 \phi_0^2 [2\rho(\tau\mathbf{v}) - \rho(\tau\mathbf{v} - \mathbf{b}) - \rho(\tau\mathbf{v} + \mathbf{b})], \quad |\mathbf{b}| \gtrsim r_F, \quad (59)$$

where $\rho(\cdot)$ is the spatial autocorrelation function of the ionospheric phase (see equation 8). From Fig. 5, we see that when $|\mathbf{b}| \lesssim r_F$ (case 1), the correlation-time ($\tau_{\text{corr}} = 2r_F/v$) is dictated by the time it takes the turbulence to cross the Fresnel-scale, and for $|\mathbf{b}| \gtrsim r_F$ the correlation time ($\tau_{\text{corr}} = 2b/v$ or $4b/v$ depending on projection) is dictated by the time it takes the turbulence to cross the baseline-length (case 2). The latter is due to the fact that the visibility phase on baseline $|\mathbf{b}|$ is dominated by plasma wave-modes of size $\sim |\mathbf{b}|$ that decorrelate on length-scale of the same order. But in the former case, the convolution with the Fresnel-exponent sets a minimum decorrelation scale (spatially) that is of the order r_F . For typical values of $\nu = 150$ MHz, $h = 300$ km, $v = 100 - 500$ km/hr for ionospheric scintillation parameters, the decorrelation time for $|\mathbf{b}| < r_F$ (≈ 300 metres) varies between 4 and 22 seconds respectively, whereas for $|\mathbf{b}| = 2$ km ($|\mathbf{b}| > r_F$) the decorrelation time varies between 30 and 150 sec for plasma motion perpendicular to the baseline and twice as much for plasma motion parallel to the baseline.

5.2 Spatial coherence

In practice, we average redundant (or near-redundant) baselines, and hence we will concern ourselves with visibility coherence between baselines-pairs that are identical (same length and orientation) but are displaced by a vector \mathbf{s} . It is straightforward to show that the coherence relationship is then identical to the one in equation 58 but with $\tau\mathbf{v}$ replaced by \mathbf{s} . This is because, laterally shifting the ionosphere by \mathbf{s} is identical to shifting the baseline by the same amount. Hence, we arrive at the following conclusion. For visibility scintillation of the point-like source flux, we again have two cases: (i) if $|\mathbf{b}| \lesssim r_F$, then redundant baseline separated by more than the Fresnel-scale (r_F) experience incoherent visibility scintillation, and (ii) for $|\mathbf{b}| \gtrsim r_F$, the separation between redundant baseline-pairs must exceed the baseline length itself for the scintillation to decorrelate. Consequently, in highly compact arrays where all baselines lie within the Fresnel length r_F , all near-redundant baselines experience coherence speckle-noise.

5.3 Frequency coherence

Analytically computing the visibility covariance between two frequencies is algebraically cumbersome, and we will restrict ourselves to heuristic arguments based on the terms in equation 31. Firstly, the overall magnitude of the effect varies as a function of frequency (via $|\tilde{\phi}(\mathbf{q})|^2$) due to the frequency-scaling of the diffractive scale. Apart from this bulk effect, we expect decorrelation on smaller bandwidths due to geometric effects. Since the interferometer-fringe spacing scales with frequency,

⁸ $\sigma_\tau^2[V(\mathbf{b})]$ is in general complex for $|\mathbf{b}| \lesssim r_F$, but the imaginary part is small compared to the real part. In Fig. 5 we plot the absolute value of $\sigma_\tau^2[V(\mathbf{b})]$.

even in the absence of scattering, we expect frequency decorrelation in the visibility on wavelength scales of $\Delta\lambda_{\text{fringe}} = d\lambda/b$: visibilities at wavelengths separated by more than $\Delta\lambda_{\text{fringe}}$ are typically not averaged coherently. An additional geometric effect is imposed by the Fresnel-filter (the sine-squared term). We can compute this by evaluating equation 41 for visibility correlation at wavelengths λ_1 and λ_2 :

$$\sigma^2 [V(b, \lambda_1, \lambda_2)] = 4 \int dq \left| \tilde{\phi}(q) \right|^2 \sin(-\pi qb + \pi \lambda_1 h q^2) \sin(-\pi qb + \pi \lambda_2 h q^2) \langle V_o(b - \lambda_1 h q) V_o^*(b - \lambda_2 h q) \rangle, \quad (60)$$

where we have assumed a sufficiently small separation between λ_1 and λ_2 , such that variation in $\left| \tilde{\phi}(q) \right|^2$ can be ignored. Using $\lambda_0 = (\lambda_1 + \lambda_2)/2$, and $\Delta\lambda = \lambda_1 - \lambda_2$, we can write

$$\sigma^2 [V(b, \lambda_1, \lambda_2)] = 4 \int dq \left| \tilde{\phi}(q) \right|^2 \langle V_o(b - \lambda_1 h q) V_o^*(b - \lambda_2 h q) \rangle [\sin^2(-\pi qb + \pi \lambda_0 h q^2) - \sin^2(\pi \Delta\lambda h q^2/2)] \quad (61)$$

which is the same as the visibility variance at λ_0 , but with a modified Fresnel-filter (sine-squared) term. The additional term in the new Fresnel-filter— $\sin^2(\pi \Delta\lambda h q^2/2)$ reaches appreciable values only for $\Delta\lambda \gtrsim 1/(2h q^2)$. Hence contribution from turbulence on spatial scales smaller than $1/q = \sqrt{2h\Delta\lambda}$ is suppressed in the visibility covariance, whereas contribution from larger scale fluctuations are mostly unaffected due to a change in wavelength. Due to the steep $-11/3$ law followed by $\left| \tilde{\phi}(q) \right|^2$, variance contribution from $\Delta\lambda \gtrsim 1/(2h q^2)$ is negligibly small for $\Delta\lambda \lesssim \lambda_0$, and we conclude that decorrelation in the Fresnel-filter term is sub-dominant to fringe-decorrelation. In the image domain, this can be thought of as the following: the frequency-decorrelation in the observed speckle pattern is mostly due to a variation in the instantaneous⁹ point-spread function (PSF) with frequency, rather than a variation in the intrinsic speckle pattern itself. Current low-frequency arrays typically have low filling factors, and suffer significant snapshot PSF decorrelation with frequency. We expect this to be a dominant cause of scintillation decorrelation in the Fourier plane (uv -plane) over $\Delta\lambda \approx d\lambda/b$, or equivalently, $\Delta\nu/\nu \approx d/b$.

6 CONCLUSIONS AND FUTURE WORK

Several new and upcoming radio-telescopes operate at low radio-frequencies ($\nu \lesssim 200$ MHz), and cater to a wide variety of science goals. The low frequencies and the accompanying wide fields-of-view require us to revisit plasma propagation effects that were earlier studied for the special case of observations of a single unresolved (or partially resolved) source at the phase-centre. We have done so in this paper, and have arrived at the following conclusions. Propagation through a plasma (like the ionosphere) imposes a frequency, time, and position dependent phase. The inherent randomness in plasma turbulence results in a stochastic visibility scintillation effect. We have derived expressions (equation 31) for the ensuing visibility variance for a wide field of view (several to tens of degrees) radio interferometer. Using these expressions, we show that for current low frequency arrays ($\nu \lesssim 200$ MHz) this source of uncertainty is typically larger than sky noise (Fig. 4).

The coherence time-scale for visibility scintillation of point-like sources is dictated by the time it takes for the turbulence to travel a distance $s = 2b$ or $s = 4b$ (b is the baseline length) depending on whether the bulk-velocity is perpendicular or parallel to the baseline. However, the coherence time cannot be smaller than the time it takes for the bulk motion to travel a distance of $s = 2r_F$, where r_F is the Fresnel scale. Coherence of visibility scintillation between redundant baseline pairs separated by s is similar to time-coherence on a timescale of $\tau = s/v$. Due to their low filling factors, frequency decorrelation of visibility scintillation in current arrays is mostly caused by scaling of the snapshot point-spread-function with frequency, rather than an evolution in the scintillation pattern itself.

Visibility scintillation effects are particularly relevant for experiments requiring high dynamic range measurements such as observations of the highly redshifted 21-cm signal from the Cosmic Dawn and Reionization epochs. In this paper, we have made the first inroads into assessing the level of visibility scintillation in such experiments. The final uncertainty due to ionospheric propagation effects depends on the telescope geometry, and the extent to which calibration algorithms can mitigate the above effects. We reserve a detailed discussion of these issues to a forthcoming paper.

REFERENCES

- Born M., Wolf E., 1999, Principles of Optics. Cambridge Univ. Press
- Cronyn W. M., 1972, ApJ, 174, 181
- Goodman J., Narayan R., 1989, MNRAS, 238, 995

⁹ Instantaneous here must be interpreted as within typical time-decorrelation scale.

- Hewish A., 1952, Royal Society of London Proceedings Series A, 214, 494
 Koopmans L. V. E., 2010, The Astrophysical Journal, 718, 963
 Mercier R. P., Budden K. G., 1962, Proceedings of the Cambridge Philosophical Society, 58, 382
 Parsons A. R. et al., 2010, AJ, 139, 1468
 Pearson T. J., Readhead A. C. S., 1984, ARA&A, 22, 97
 Rufenach C. L., 1972, J. of Geophys. Res., 77, 4761
 Salpeter E. E., 1967, ApJ, 147, 433
 Smith F. G., 1950, Nature, 165, 422
 Swarup G., Ananthakrishnan S., Kapahi V. K., Rao A. P., Subrahmanya C. R., Kulkarni V. K., 1991, Current Science, 60, 95
 Taylor A. R., Braun R., eds., 1999, Science with the Square Kilometer Array : a next generation world radio observatory
 Tingay S. J. et al., 2013, PASA, 30, 7
 van Haarlem M. P. et al., 2013, A&A, 556, A2
 von Karman T., 1948, Proc. Natl. Acad. Sci. U.S.A., 34, 530
 Wheelon A. D., 2001, Electromagnetic scintillation. I. Geometrical optics. Cambridge Univ. Press
 Wheelon A. D., 2003, Electromagnetic scintillation. Vol.2: Weak scattering. Cambridge University Press
 Windhorst R. A., Miley G. K., Owen F. N., Kron R. G., Koo D. C., 1985, ApJ, 289, 494

APPENDIX A: SINGLE SOURCE VISIBILITY EXPECTATION

Using equation 24, the single source visibility expectation is

$$\langle V(\mathbf{b}, \mathbf{l}) \rangle = \frac{\exp[i2\pi\mathbf{b} \cdot \mathbf{l}/\lambda]}{\lambda^2 h^2} \int \int d^2\mathbf{x}_1 d^2\mathbf{x}_2 \exp\left[\frac{i\pi}{\lambda h}(\mathbf{x}_1^2 - \mathbf{x}_2^2)\right] \cdot \langle \exp[i(\phi(\mathbf{x}_1 + h\mathbf{l}) - \phi(\mathbf{x}_2 + h\mathbf{l} + \mathbf{b}))] \rangle \quad (\text{A1})$$

To compute the expectation on ionospheric phases we will use the following theorem: If a_k are scalars, and ϕ_k are Gaussian random variables, then

$$\left\langle \exp\left[i \sum_k a_k \phi_k\right] \right\rangle = \exp\left[-\frac{1}{2} \sum_k \sum_m a_k a_m \langle \phi_k \phi_m \rangle\right] \quad (\text{A2})$$

The visibility expectation is then

$$\langle V(\mathbf{b}, \mathbf{l}) \rangle = \frac{\exp[i2\pi\mathbf{b} \cdot \mathbf{l}/\lambda]}{\lambda^2 h^2} \int \int d^2\mathbf{x}_1 d^2\mathbf{x}_2 \exp\left[\frac{i\pi}{\lambda h}(\mathbf{x}_1^2 - \mathbf{x}_2^2)\right] \exp[-\phi_0^2(1 - \rho(\mathbf{x}_1 - \mathbf{x}_2 - \mathbf{b}))] \quad (\text{A3})$$

Making the change of integration variables from $\mathbf{x}_1, \mathbf{x}_2$ to \mathbf{u}, \mathbf{v} where $\mathbf{u} = (\mathbf{x}_1 + \mathbf{x}_2)/\sqrt{2}$ and $\mathbf{v} = (\mathbf{x}_1 - \mathbf{x}_2)/\sqrt{2}$, we get

$$\langle V(\mathbf{b}, \mathbf{l}) \rangle = \frac{\exp[i2\pi\mathbf{b} \cdot \mathbf{l}/\lambda]}{\lambda^2 h^2} \int \int d^2\mathbf{u} d^2\mathbf{v} \exp\left[\frac{i\pi}{\lambda h}\mathbf{u} \cdot \mathbf{v}\right] \exp[-\phi_0^2(1 - \rho(\mathbf{v}\sqrt{2} - \mathbf{b}))] \quad (\text{A4})$$

The integration with respect to \mathbf{u} is straightforward and yields, $\lambda^2 h^2 \delta(\mathbf{v})$, where $\delta(\cdot)$ is the 2-dimensional Dirac-delta function. The integration with respect to \mathbf{v} returns the integrand at $\mathbf{v} = \mathbf{0}$:

$$\langle V(\mathbf{b}, \mathbf{l}) \rangle = \exp[i2\pi\mathbf{b} \cdot \mathbf{l}/\lambda] \exp[-\phi_0^2(1 - \rho(\mathbf{b}))] \quad (\text{A5})$$

The result can be written in terms of the structure function $\mathcal{D}(\mathbf{b}) = 2\phi_0^2(1 - \rho(\mathbf{b}))$ as

$$\langle V(\mathbf{b}, \mathbf{l}) \rangle = \exp[i2\pi\mathbf{b} \cdot \mathbf{l}/\lambda] \exp\left[-\frac{1}{2}\mathcal{D}(\mathbf{b})\right]. \quad (\text{A6})$$

APPENDIX B: TWO-SOURCE VISIBILITY CO-VARIANCE

We define the two-source visibility as

$$\sigma^2[V_{\text{pp}}(\mathbf{b}, \mathbf{l}_a, \mathbf{l}_b)] = \langle V(\mathbf{b}, \mathbf{l}_a) V^*(\mathbf{b}, \mathbf{l}_b) \rangle - \langle V(\mathbf{b}, \mathbf{l}_a) \rangle \langle V(\mathbf{b}, \mathbf{l}_b) \rangle^*. \quad (\text{B1})$$

The first term is basically the mutual-coherence between visibilities on the same baseline due to two sources in the sky:

$$\begin{aligned} \langle V(\mathbf{b}, \mathbf{l}_a) V^*(\mathbf{b}, \mathbf{l}_b) \rangle &= \frac{\exp[i2\pi\mathbf{b} \cdot \Delta\mathbf{l}]}{\lambda^4 h^4} \int \int \int \int d^2\mathbf{x}_1 d^2\mathbf{x}_2 d^2\mathbf{x}_3 d^2\mathbf{x}_4 \exp\left[\frac{i\pi}{\lambda h}(\mathbf{x}_1^2 - \mathbf{x}_2^2 - \mathbf{x}_3^2 + \mathbf{x}_4^2)\right] \\ &\quad \langle \exp[i(\phi(\mathbf{x}_1 + h\mathbf{l}_a) - \phi(\mathbf{x}_2 + h\mathbf{l}_a + \mathbf{b}) - \phi(\mathbf{x}_3 + h\mathbf{l}_b) + \phi(\mathbf{x}_4 + h\mathbf{l}_b + \mathbf{b}))] \rangle. \end{aligned} \quad (\text{B2})$$

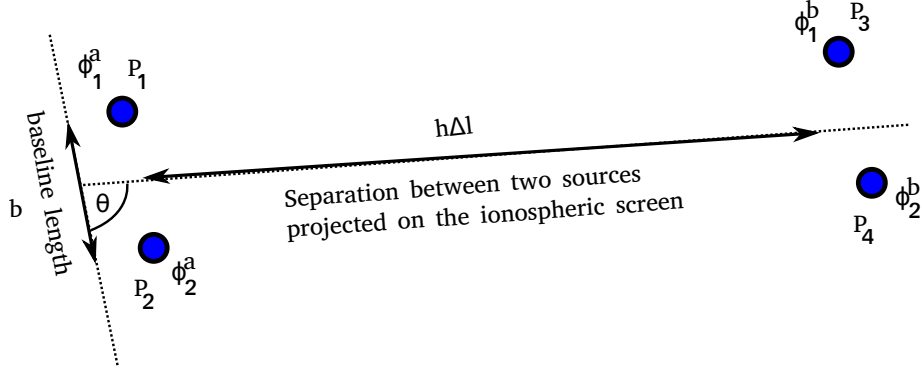


Figure B1. Sketch comparing the baseline length to the projected separation (on the ionospheric screen) of the baseline for two sources

The expectation in the above equation is the 4-point phase coherence on the ionospheric screen. Fig. B1 depicts the geometry of the 4-points that correspond to the ‘pierce-points’ on the ionospheric plane of the rays that go from the two antennas towards the two sources. The expectation in the above equation depends on the phase structure on all 16 pairs that can be drawn from 4 pierce-points, and can be written using equation A2 as

$$\langle V(\mathbf{b}, l_a) V^*(\mathbf{b}, l_b) \rangle = \frac{\exp[i2\pi \mathbf{b} \cdot \Delta \mathbf{l}]}{\lambda^4 h^4} \int \int \int \int d^2 \mathbf{x}_1 d^2 \mathbf{x}_2 d^2 \mathbf{x}_3 d^2 \mathbf{x}_4 \exp \left[\frac{i\pi}{\lambda h} (\mathbf{x}_1^2 - \mathbf{x}_2^2 - \mathbf{x}_3^2 + \mathbf{x}_4^2) \right] \left(\exp \left[-\frac{\phi_0^2(\psi)}{2} \right] \right), \quad (\text{B3})$$

(B4)

where ψ is given by

$$\psi = 4 - 2(\rho(\mathbf{x}_{12} + \mathbf{b}) + \rho(\mathbf{x}_{13} + h\Delta \mathbf{l}) - \rho(\mathbf{x}_{14} + h\Delta \mathbf{l} - \mathbf{b}) - \rho(\mathbf{x}_{23} + h\Delta \mathbf{l} + \mathbf{b}) + \rho(\mathbf{x}_{24} + h\Delta \mathbf{l}) + \rho(\mathbf{x}_{34} - \mathbf{b})), \quad (\text{B5})$$

where we have used the short-hand notation $\mathbf{x}_{ij} = \mathbf{x}_i - \mathbf{x}_j$. The integrations may not be carried out analytically. Since we are in the weak scattering regime, we may proceed by Taylor expanding the exponent about 0 as

$$\exp \left[-\frac{\phi_0^2 \psi}{2} \right] \approx 1 - \frac{\phi_0^2 \psi}{2} \quad (\text{B6})$$

Now that the exponent has been linearised, equation B3 reduces to a sum of integrals, with each integral being a Fresnel integral of a two-point correlation function $\rho(\cdot)$. All but two of the integrals can be evaluated using a procedure similar to the one in Appendix A, and we get

$$\langle V(\mathbf{b}, l_a) V^*(\mathbf{b}, l_b) \rangle = \exp[i2\pi \mathbf{b} \cdot \Delta \mathbf{l}] [1 - 2\phi_0^2 (1 - \rho(\mathbf{b})) + \phi_0^2 (2\rho(h\Delta \mathbf{l}) - T_1 - T_2)], \quad (\text{B7})$$

where T_1 and T_2 have $\rho(\Delta \mathbf{x}_{23} + h\Delta \mathbf{l} + \mathbf{b})$ and $\rho(\Delta \mathbf{x}_{14} + h\Delta \mathbf{l} - \mathbf{b})$ as the integrands respectively. T_1 can be further reduced as follows.

$$T_1 = \left[\frac{1}{\lambda^2 h^2} \int \int d^2 \mathbf{x}_1 d^2 \mathbf{x}_4 \exp \left[\frac{i\pi}{\lambda h} (\mathbf{x}_1^2 + \mathbf{x}_4^2) \right] \right] \cdot \left[\frac{1}{\lambda^2 h^2} \int \int d^2 \mathbf{x}_2 d^2 \mathbf{x}_3 \exp \left[\frac{i\pi}{\lambda h} (-\mathbf{x}_2^2 - \mathbf{x}_3^2) \right] \rho(\Delta \mathbf{x}_{23} + h\Delta \mathbf{l} + \mathbf{b}) \right]. \quad (\text{B8})$$

The integrals with respect to \mathbf{x}_1 and \mathbf{x}_4 are both Fresnel integrals in the absence of any phase modulation, and each of them reduces to i , and their product is -1 . To compute the integrals with respect to \mathbf{x}_2 and \mathbf{x}_3 , we make the change of variables: $\mathbf{u} = (\mathbf{x}_2 - \mathbf{x}_3)/\sqrt{2}$, $\mathbf{v} = (\mathbf{x}_2 + \mathbf{x}_3)/\sqrt{2}$ to get

$$T_1 = -\frac{1}{\lambda^2 h^2} \int \int d^2 \mathbf{u} d^2 \mathbf{v} \exp \left[\frac{i\pi}{\lambda h} (-\mathbf{u}^2 - \mathbf{v}^2) \right] \rho(\sqrt{2}\mathbf{u} + h\Delta \mathbf{l} + \mathbf{b}). \quad (\text{B9})$$

The integration with respect to \mathbf{v} is again a Fresnel integral with no phase modulations and reduces to $-i$. Hence, we get

$$T_1 = \frac{i}{\lambda h} \int d^2 \mathbf{u} \exp \left[\frac{i\pi}{\lambda h} (-\mathbf{u}^2) \right] \rho(\sqrt{2}\mathbf{u} + h\Delta \mathbf{l} + \mathbf{b}). \quad (\text{B10})$$

We are unable to proceed analytically any further. However, equation B10 is a convolution between two functions at lag $\mathbf{b} + h\Delta \mathbf{l}$, and using the convolution theorem we can write

$$T_1 = \frac{1}{\phi_0^2} \int d^2 \mathbf{q} \exp[i2\pi \mathbf{q} \cdot (\mathbf{b} + h\Delta \mathbf{l})] \left| \tilde{\phi}(\mathbf{q}) \right|^2 \exp[i2\pi \lambda h \mathbf{q}^2], \quad (\text{B11})$$

where \mathbf{q} and $h\Delta\mathbf{l}$ form a Fourier conjugate pair, $|\tilde{\phi}(\mathbf{q})|^2$ is the Fourier transform of $\phi_0^2\rho(\mathbf{u})$, and $\exp[i2\pi\lambda h\mathbf{q}^2]$ is the Fourier transform of $i/(\lambda h)\exp[\frac{i\pi}{\lambda h}(-\mathbf{u}^2)]$. Using a similar procedure, T_2 can be reduced to

$$T_2 = \frac{1}{\phi_0^2} \int d^2\mathbf{q} \exp[-i2\pi\mathbf{q} \cdot (\mathbf{b} - h\Delta\mathbf{l})] |\tilde{\phi}(\mathbf{q})|^2 \exp[-i2\pi\lambda h\mathbf{q}^2]. \quad (\text{B12})$$

Hence $T_1 + T_2$ is given by

$$T_1 + T_2 = \frac{1}{\phi_0^2} \int d^2\mathbf{q} |\tilde{\phi}(\mathbf{q})|^2 \exp[i2\pi h\mathbf{q} \cdot \Delta\mathbf{l}] 2 \cos(2\pi\mathbf{q} \cdot \mathbf{b} + 2\pi\lambda h\mathbf{q}^2), \quad (\text{B13})$$

Collecting all terms, we get

$$\langle V(\mathbf{b}, l_a) V^*(\mathbf{b}, l_b) \rangle = \exp[i2\pi\mathbf{b} \cdot \Delta\mathbf{l}] \left[1 - 2\phi_0^2 \left(1 - \rho(\mathbf{b}) - \rho(h\Delta\mathbf{l}) + \int d^2\mathbf{q} |\tilde{\phi}(\mathbf{q})|^2 \exp[-i\pi h\mathbf{q} \cdot \Delta\mathbf{l}] \cos(-2\pi\mathbf{q} \cdot \mathbf{b} + 2\pi\lambda h\mathbf{q}^2) \right) \right], \quad (\text{B14})$$

where we have made the substitutions $\mathbf{q} \rightarrow -\mathbf{q}$ to preserve the sign convention in the Fourier transform with respect to \mathbf{q} . Writing $\phi_0^2\rho(h\Delta\mathbf{l})$ in terms of its Fourier transform, taking in into the integral, and using the trigonometric half-angle formula, we get

$$\langle V(\mathbf{b}, l_a) V^*(\mathbf{b}, l_b) \rangle = \exp[i2\pi\mathbf{b} \cdot \Delta\mathbf{l}] \left[1 - 2\phi_0^2 + 2\phi_0^2\rho(\mathbf{b}) + 4 \int d^2\mathbf{q} \exp[-i2\pi h\mathbf{q} \cdot \Delta\mathbf{l}] |\tilde{\phi}(\mathbf{q})|^2 \sin^2(-\pi\mathbf{q} \cdot \mathbf{b} + \pi\lambda h\mathbf{q}^2) \right] \quad (\text{B15})$$

The second term in equation B1 can be evaluated using equation A6 as

$$\langle V(\mathbf{b}, l_a) \rangle \langle V(\mathbf{b}, l_a) \rangle^* = \exp[i2\pi\mathbf{b} \cdot \Delta\mathbf{l}/\lambda] \exp[-\mathcal{D}(\mathbf{b})] = \exp[i2\pi\mathbf{b} \cdot \Delta\mathbf{l}/\lambda] \exp[-2\phi_0^2(1 - \rho(\mathbf{b}))] \quad (\text{B16})$$

We may Taylor expand the exponent in the weak-scattering limit to get

$$\langle V(\mathbf{b}, l_a) \rangle \langle V(\mathbf{b}, l_a) \rangle^* = \exp[i2\pi\mathbf{b} \cdot \Delta\mathbf{l}/\lambda] [1 - 2\phi_0^2 + 2\phi_0^2\rho(\mathbf{b})] \quad (\text{B17})$$

Substituting equations B15 and B17, in equation B1, we get the expression for the two-source visibility co-variance:

$$\sigma^2[V(\mathbf{b}, l_a, l_b)] = 4 \exp[i2\pi\mathbf{b} \cdot \Delta\mathbf{l}] \int d^2\mathbf{q} \exp[-i2\pi h\mathbf{q} \cdot \Delta\mathbf{l}] |\tilde{\phi}(\mathbf{q})|^2 \sin^2(-\pi\mathbf{q} \cdot \mathbf{b} + \pi\lambda h\mathbf{q}^2) \quad (\text{B18})$$

The two-source visibility variance for the pierce-point approximation may be computed by discounting the Fresnel-integrations in equation B3, or in other words, by extracting the value of the integral at $\mathbf{x}_1 = \mathbf{x}_2 = \mathbf{x}_3 = \mathbf{x}_4 = \mathbf{0}$. The computations are straightforward, and yield

$$\sigma^2[V_{\text{pp}}(\mathbf{b}, l_a, l_b)] = 4 \exp[i2\pi\mathbf{b} \cdot \Delta\mathbf{l}] \int d^2\mathbf{q} \exp[-i2\pi h\mathbf{q} \cdot \Delta\mathbf{l}] |\tilde{\phi}(\mathbf{q})|^2 \sin^2(\pi\mathbf{q} \cdot \mathbf{b}) \quad (\text{B19})$$